

Gaussian Splashing: Dynamic Fluid Synthesis with Gaussian Splatting

YUTAO FENG*, University of Utah, USA and Zhejiang University, China

XIANG FENG*, Zhejiang University, China

YINTONG SHANG, University of Utah, USA

YING JIANG, UCLA, USA

CHANG YU, UCLA, USA

ZESHUN ZONG, UCLA, USA

TIANJIA SHAO, Zhejiang University, China

HONGZHI WU, Zhejiang University, China

KUN ZHOU, Zhejiang University, China

CHENFANFU JIANG, UCLA, USA

YIN YANG, University of Utah, USA



Fig. 1. **Splashing LEGO.** Gaussian Splashing (GSP) is a unified framework combining position-based dynamics and 3D Gaussian Splatting (3DGS). By leveraging their coherent point-based representations, GSP delivers high-quality rendering for novel dynamic views involving interacting solids and fluids. GSP enables a variety of interesting effects and new human-computer interaction modalities that are not available with existing NeRF/3DGS based systems. The teaser figure showcases the interaction between a LEGO excavator and the splashing waves. There are 334,815 solid Gaussian kernels and 280,000 fluid Gaussian kernels. Those volumetric Gaussians not only capture nonlinear dynamics of two-way coupled fluids and solids but can also be rasterized to realistically render with both diffuse and specular shading. GSP re-engineers several state-of-the-art techniques from neural surface reconstruction, specular-aware Gaussian shader, position-based tension, and AI inpainting to ensure the quality of both simulation and rendering with 3DGS.

We demonstrate the feasibility of integrating physics-based animations of solids and fluids with 3D Gaussian Splatting (3DGS) to create novel effects in virtual scenes reconstructed using 3DGS. Leveraging the coherence of the Gaussian splatting and position-based dynamics (PBD) in the underlying representation, we manage rendering, view synthesis, and the dynamics of solids and fluids in a cohesive manner. Similar to Gaussian shader, we enhance each Gaussian kernel with an added normal, aligning the kernel’s orientation with the surface normal to refine the PBD simulation. This approach effectively eliminates spiky noises that arise from rotational deformation in solids. It also allows us to integrate physically based rendering to augment the dynamic surface reflections on fluids. Consequently, our

framework is capable of realistically reproducing surface highlights on dynamic fluids and facilitating interactions between scene objects and fluids from new views. For more information, please visit our project page at <https://amysteriouscat.github.io/GaussianSplashing/>.

1 INTRODUCTION

Visualization and reconstruction of 3D scenes have been the core of 3D graphics and vision. Recent development of learning-based techniques such as the neural radiance fields (NeRFs) [Mildenhall et al. 2020] sheds new light on this topic. NeRF casts the reconstruction pipeline as a training procedure and delivers state-of-the-art results by encapsulating the color, texture, and geometry of the 3D scene into an implicit MLP net. Its superior convenience and efficacy inspire many follow-ups e.g., with improved visual quality [Liu et al. 2020], faster performance [Garbin et al. 2021; Yu et al. 2021], and sparser inputs [Jain et al. 2021; Yuan et al. 2022a]. NeRF is designed for ray tracing, which is less suitable for real-time or interactive applications unless dedicated compression or acceleration methods are employed e.g., with NGP encoding [Müller et al. 2022]. 3D Gaussian splatting (3DGS) [Kerbl et al. 2023] provides an elegant alternative. As the name suggests, 3DGS learns a collection of Gaussian kernels

*Both authors contributed equally to this research.

Authors’ addresses: Yutao Feng, fytao0n@gmail.com, University of Utah, Salt Lake City, Utah, USA and Zhejiang University, Hangzhou, Zhejiang, China; Xiang Feng, xfeng.cg@gmail.com, Zhejiang University, Hangzhou, Zhejiang, China; Yintong Shang, University of Utah, Salt Lake City, Utah, USA, shayito_@outlook.com; Ying Jiang, UCLA, Los Angeles, USA, California, anajymua@gmail.com; Chang Yu, UCLA, Los Angeles, USA, California, g1n0st@live.com; Zeshun Zong, UCLA, Los Angeles, USA, California, zeshunzong@math.ucla.edu; Tianjia Shao, tjshao@zju.edu.cn, Zhejiang University, Hangzhou, Zhejiang, China; Hongzhi Wu, hwwu@acm.org, Zhejiang University, Hangzhou, Zhejiang, China; Kun Zhou, kunzhou@acm.org, Zhejiang University, Hangzhou, Zhejiang, China; Chenfanfu Jiang, UCLA, Los Angeles, USA, California, chenfanfu.jiang@gmail.com; Yin Yang, University of Utah, Salt Lake City, Utah, USA, yangzzyy@gmail.com.

from the input images. Apart from NeRF, a novel view of the scene from an unseen camera pose is generated using rasterization with the tile-splatting technique. Therefore, fast rendering with 3DGS is feasible.

It is noted that Gaussian kernels not only serve as a good rendering agent but also explicitly encode rich information of the scene geometry. This feature suggests 3DGS a good candidate for dynamic scenes [Duisterhof et al. 2023; Wu et al. 2023; Yang et al. 2023], animated avatars [Moreau et al. 2023; Zielonka et al. 2023], or simulated physics [Xie et al. 2023]. We expand on this intuition, enhancing the current 3DGS ecosystem by injecting physics-based fluid and solid interactions into a 3DGS scene. This appears straightforward at first sight. Since 3DGS kernels are essentially a collection of ellipsoids, they can be used for the discretization of the fluid and solid dynamics just as position-based dynamics [Macklin et al. 2016], oriented particles [Müller and Chentanez 2011] or other particle-based simulation techniques. Unfortunately, a simple combination of those techniques does not yield the results expected. Large rotational deformation of the solid objects affects the splatting results with sharp and spiky noises. During fluid motion, fluid particles undergo substantial positional shifts, moving from the inside to the outside or vice versa. Fluids are both translucent and specular. The vanilla 3DGS simplifies the composition of the light field without well-defined appearance properties. This limitation makes fluid rendering cumbersome with 3DGS.

This paper presents a system namely Gaussian Splashing (GSP), a 3DGS-based framework that enables realistic interactions between solid objects and fluids in a physically meaningful way, and thus generates two-way coupled fluids-solids dynamics in novel views. GSP integrates Lagrangian fluid and 3DGS scenes through a unified framework of position-based dynamics (PBD) [Macklin et al. 2016; Müller et al. 2007]. We follow a recent contribution of Gaussian shader [Jiang et al. 2023] to augment Gaussian kernels with additional environmental information so that specular shading can be dynamically synthesized along with the fluid’s movement. For solid objects, GSP uses an anisotropy loss to cap the stretching ratio during 3DGS training and mitigate the rendering artifacts induced by rotational deformation. We approximate the normal of a fluid kernel based on the surface tension if it is near the fluid surface. For scattered fluid droplets, we resort to a depth volume rendered via the current camera pose to estimate the normal information [van der Laan et al. 2009]. GSP is versatile, due to the flexibility of PBD. It handles deformable bodies, rigid objects, and fluid dynamics in a unified way. While it is possible to incorporate more complicated constitutional models as in [Feng et al. 2023] and [Li et al. 2023]. We found that PBD-based simulation suffices in many situations. We further augment GSP with an image-space segmentation module to select objects of interest from the 3DGS scene. We exploit the latest generative AI to fill the missing pixels to enable interesting physics-based scene editing.

In a nutshell, GSP leverages a unified, volumetric, particle-based representation for rendering, 3D reconstruction, view synthesis, and dynamic simulation. It contributes a novel 3D graphics/vision system that allows natural and realistic solid-fluid interactions in real-world 3DGS scenes. This is achieved by carefully engineering the pipeline to overcome the limitations of the vanilla 3DGS.

GSP could enable a variety of intriguing effects and new human-computer interaction modalities in a diverse range of applications. For instance, one can pour water to flood the scene, floating the objects within, or directly liquefy an object, just as in science fiction. Fig. 1 showcases the dynamic interaction between a LEGO excavator and the splashing waves. There are 334,815 solid Gaussian kernels and 280,000 fluid Gaussian kernels. Through the two-way coupling dynamics, the excavator is animated to surf on the splashing waves.

2 RELATED WORK

Dynamic neural radiance field. Dynamic neural radiance fields generalize the original NeRF system to capture time-varying scenes e.g., by decomposing time-dependent neural fields into an inverse displacement field and canonical time-invariant neural fields [Park et al. 2021a,b; Treitschk et al. 2021; Weng et al. 2022], or estimating the time-continuous 3D motion field [Du et al. 2021; Gao et al. 2021; Guo et al. 2023; Li et al. 2021; Liu et al. 2022; Pumarola et al. 2021; Xian et al. 2021] with an added temporal dimension. Existing arts enable direct edits of NeRF reconstructions [Bao et al. 2023; Dong and Wang 2023; Jiang et al. 2022]. In dynamic scenes, the rendering process needs to trace deformed sample points back to rest-shape space to correctly retrieve the color/texture information [Peng et al. 2022; Qiao et al. 2023; Xu and Harada 2022; Yuan et al. 2022b]. They often extract a mesh/grid from the NeRF volume. It is also possible to integrate physical simulation with NeRF using meshless methods [Feng et al. 2023; Li et al. 2023]. Point NeRF [Xu et al. 2022] and 3DGS [Kerbl et al. 2023] offer a different perspective to scene representation explicitly using points/Gaussian kernels to encode the scene. The success of 3DGS has inspired many studies to transplant techniques for dynamic NeRF to 3DGS [Liang et al. 2023b; Wu et al. 2023; Xu et al. 2023]. They incorporate learning-based deformation and editing techniques to reconstruct or generate dynamics of NeRF scenes. It is noteworthy that a recent work from Xie et al. [2023] integrates physical simulation with 3DGS, leveraging the unified proxy for both simulating and rendering.

Lagrangian fluid simulation. Lagrangian fluid simulation tracks fluid motion using individual particles as they traverse the simulation domain. A seminal approach within this domain is smoothed particle hydrodynamics (SPH) [Monaghan 1992], which solves fluid dynamics equations by assessing the influence of neighboring particles. Despite its efficacy, SPH, particularly in its standard and weakly compressible forms (WCSPH) [Becker and Teschner 2007], suffers from parameter sensitivity, e.g., kernel radius and time-step size for stiff equations. To relax the time-step restriction, predictive-corrective incompressible SPH (PCISPH) [Solenthaler and Pajarola 2009] iteratively corrects pressure based on the density error. Similarly, position-based dynamics [Müller et al. 2007] provides a robust method of solving a system of non-linear constraints using Gauss-Seidel iterations by updating particle positions directly, which can also be employed in fluid simulation [Macklin and Müller 2013] with improved stability. Furthermore, surface tension can also be generated [Xing et al. 2022] using the position-based iterative solver by tracking surface particles and solving constraints on them to minimize the surface area.

Reflective object rendering. Achieving precise rendering of reflective surfaces relies on accurately estimating scene illumination, such as environmental light, and material properties like bidirectional reflectance distribution function (BRDF). This task falls under the domain of inverse rendering [Barron and Malik 2014; Nimier-David et al. 2019]. Some NeRF-related methodologies disentangle the visual appearance into lighting and material properties, which can jointly optimize environmental illumination, surface geometry, and material [Bi et al. 2020; Boss et al. 2021a,b; Srinivasan et al. 2021; Zhang et al. 2021a,b]. Other NeRF studies [Kang et al. 2021; Liang et al. 2023a, 2022; Liu et al. 2023] aim to enhance the accuracy of the normal estimation in physically based rendering (PBR). Nevertheless, these efforts face challenges such as time-consuming training and slow rendering speed. On the contrary, 3DGS naturally offers a good normal estimation as the shortest axis of the Gaussian kernel [Guédon and Lepetit 2023; Jiang et al. 2023]. Following this idea, it is possible to achieve high-quality rendering of reflective objects and training efficiency simultaneously [Jiang et al. 2023].

Point-based rendering. Point-based rendering has been an active topic in computer graphics since the 1980s [Levoy and Whitted 1985]. The simplest method [Grossman and Dally 1998] renders a set of points with a fixed size. It suffers from holes and relies on post-processing steps such as hole-filling [Grossman and Dally 1998; Pintus et al. 2011] to correct the resulting rendering. An improvement is to use ellipsoids instead of volume-less points. This strategy is usually referred to as *splatting* [Zwicker et al. 2001]. The ellipsoids are rendered with a Gaussian alpha-mask to eliminate visible artifacts between neighboring splats and then combined by a normalizing blend function [Alexa et al. 2004; Zwicker et al. 2001]. Point-based rendering well synergizes with Lagrangian fluid rendering, enabling the calculation of fluid thickness and depth through splatting. This approach [van der Laan et al. 2009] achieves fluid rendering at an impressive real-time speed. Further extensions to splatting aim to automatically compute the shape and color of ellipsoids, for example, auto splats [Childs et al. 2012]. With the development of deep learning in recent years, learning-based approaches improve the image quality of splatting [Bui et al. 2018; Yang et al. 2020]. 3DGS [Kerbl et al. 2023] has introduced this technique into 3D reconstruction, enabling high-quality real-time novel view synthesis for reconstructed scenes. A natural idea is to combine 3DGS with fluid rendering, enabling interaction between reconstructed scenes and dynamic fluids.

3 BACKGROUND

To make our paper self-contained, we start with a brief review of PBD and 3DGS on which our pipeline is built. More detailed discussions are available in the relevant literature e.g., [Jiang et al. 2023; Kerbl et al. 2023; Macklin et al. 2016; Müller et al. 2007].

3.1 Position-based Dynamics

PBD/XPBD treats a dynamic system as a set of N vertices and M constraints. This perspective offers an easy and efficient simulation modality, converting the variational optimization to the so-called constraint projections. Specifically, XPBD considers the total system potential U as a quadratic form of all the constraints $C(\mathbf{x}) =$

$[C_1(\mathbf{x}), C_2(\mathbf{x}), \dots, C_M(\mathbf{x})]^\top$ such that $U = \frac{1}{2} C^\top(\mathbf{x}) \boldsymbol{\alpha}^{-1} C(\mathbf{x})$. Here, $\boldsymbol{\alpha}$ is the compliance matrix i.e., the inverse of the constraint stiffness. XPBD estimates an update of constraint force (i.e., the multiplier) $\Delta \boldsymbol{\lambda}$ by solving:

$$[\Delta t^2 \nabla C(\mathbf{x}) \mathbf{M}^{-1} \nabla C^\top(\mathbf{x}) + \boldsymbol{\alpha}] \Delta \boldsymbol{\lambda} = -\Delta t^2 C(\mathbf{x}) - \boldsymbol{\alpha} \boldsymbol{\lambda}, \quad (1)$$

where Δt is the time step size, and \mathbf{M} is the lumped mass matrix. The update of the primal variable $\Delta \mathbf{x}$ can then be computed as:

$$\Delta \mathbf{x} \leftarrow \mathbf{M}^{-1} \nabla C^\top(\mathbf{x}) \Delta \boldsymbol{\lambda}. \quad (2)$$

The parallelization of XPBD is enabled with a Gauss-Seidel-like scheme, which computes $\Delta \boldsymbol{\lambda}_j$ at each constraint C_j independently:

$$\Delta \boldsymbol{\lambda}_j \leftarrow \frac{-\Delta t^2 C_j(\mathbf{x}) - \boldsymbol{\alpha}_j}{\Delta t^2 \nabla C_j \mathbf{M}^{-1} \nabla C_j^\top + \boldsymbol{\alpha}_j}. \quad (3)$$

We note that such constraint-projection-based simulation naturally synergizes with 3DGS. It is also versatile and can deal with a wide range of physical problems such as fluid [Macklin and Müller 2013; Xing et al. 2022], rigid bodies [Müller et al. 2020], or hyperelastic objects [Macklin and Müller 2021].

3.2 3D Gaussian Splatting

3D Gaussian Splatting (3DGS) is a learning-based rasterization technique for 3D scene reconstruction and novel view synthesis. 3DGS encodes a radiance field using a set of Gaussian kernels \mathcal{P} with trainable parameters $\{x_p, \sigma_p, A_p, c_p\}$ for $p \in \mathcal{P}$, where x_p , σ_p , A_p and c_p represent the center, opacity, covariance matrix, and color function of each kernel. To generate a scene render, 3DGS projects these kernels onto the imaging plane according to the viewing matrix and blends their colors based on the opacity and depth. The final color of the i -th pixel is computed as:

$$c_i = \sum_k G_k(i) \sigma_k c_k(\mathbf{r}_i) \prod_{j=1}^{k-1} (1 - G_j(i) \sigma_j). \quad (4)$$

Here, all the kernels are re-ordered based on the z -values at kernel centers under the current view. $G_k(i)$ denotes the 2D Gaussian weight of the k -th kernel at pixel i , and \mathbf{r}_i is the view direction from camera to pixel i . The color functions only depend on the viewing direction.

Gaussian Shader [Jiang et al. 2023] further enhances 3DGS by incorporating additional trainable material parameters for kernel p such as diffuse \mathbf{d}_p , specular \mathbf{s}_p , roughness ρ_p , and normal \mathbf{n}_p , along with a global environment map. It fuses more information into the kernel's color:

$$c_p(\mathbf{r}_i) = \mathbf{d}_p + \mathbf{s}_p \odot L_s(\mathbf{r}_i, \mathbf{n}_p, \rho_p), \quad (5)$$

where $L_s(\mathbf{r}_i, \mathbf{n}_p, \rho_p)$ is the specular light for the kernel along \mathbf{r}_i given the normal and roughness of the kernel. It can be pre-filtered into multiple mip maps. The symbol \odot denotes the element-wise multiplication.

4 METHOD

As shown in Fig. 2, the input of our system is a collection of images of a given 3D scene taken from different viewpoints. We separate foreground objects and the image background for all the inputs and extract the surface of masked objects. We apply an anisotropy loss

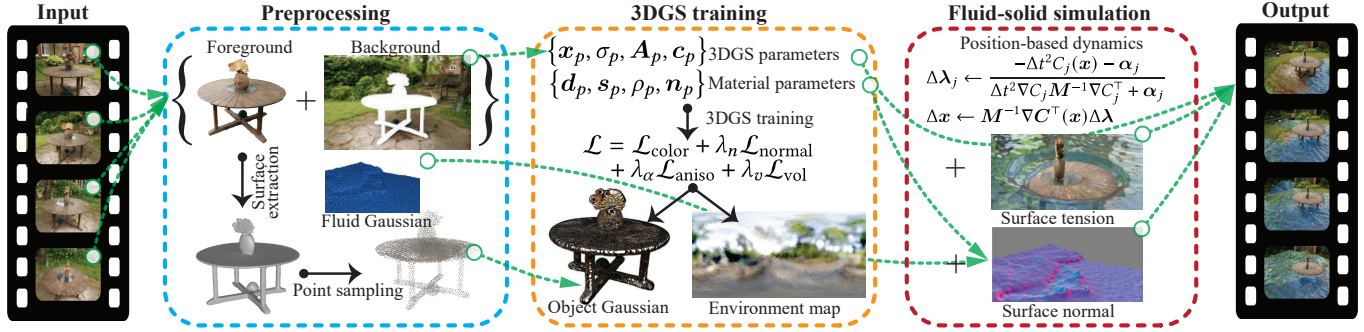


Fig. 2. **An overview of GSP pipeline.** The input to our system comprises multi-view images that capture a 3D scene. During the preprocessing stage, foreground objects are isolated and reconstructed. This is followed by point sampling to facilitate scene discretization for PBD simulation and Gaussian rendering. We train the Gaussian kernels using differentiable 3DGS, which takes into account appearance materials and lighting conditions. These kernels are animated using PBD, in conjunction with fluid particles, to tackle the dynamics of both solids and fluids within the scene. Finally, the dynamic scene is rendered into images. This rendering process includes detailed modeling of specular reflections, thereby providing visually accurate representations of the simulated interactions between solids and fluids.

to mitigate undesired splatting render to prevent over-stretching kernels when training 3DGS for the solid object. Doing so mitigates the rendering artifacts near the surface of solid models. On the other hand, fluids are made of spherical Gaussians. We track the normal for surface kernels to properly synthesize specular effects by augmenting them with an environment light map. Under the PBD framework, both fluids and solids can be animated in a unified way based on local constraint projection.

4.1 Scene Discretization

Gaussian kernels serve as the primary modality for discretizing geometry and dynamics, as well as for rendering the scene from novel camera poses. We exploit the state-of-the-art deep segmentation tools [Cheng et al. 2023; Kirillov et al. 2023] to separate foreground objects of interest out of the input images and obtain a dedicated object reconstruction. It is essential to have an accurate description of object boundaries in order to properly handle the object-object interaction or fluid-solid coupling. To this end, a surface mesh is built explicitly for each segmented foreground model using NeuS [Wang et al. 2021]. NeuS extracts the zero-level set of a signed distance function corresponding to the foreground object. We find this method tends to yield a better-quality reconstruction compared with other possible alternatives.

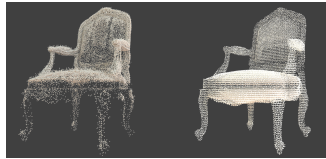


Fig. 3. **Different sampling strategies.** We compare the results of different sampling strategies: (left) fill the particle based on the density grid calculated using Gaussian kernels [Xie et al. 2023], and (right) uniformly sample within NeuS reconstruction. The point distribution generated by vanilla 3DGS is uneven, which hardly samples the legs or seat of the chair.

We use the Poisson disk sampling [Bridson 2007] to place Gaussian kernels inside the reconstructed model and regard each kernel as a mass particle for PBD simulation. In addition, we also assign kernels over the model’s surface for collision processing and fluid-solid

interaction. It is noted that existing frameworks that incorporate physics with 3DGS [Xie et al. 2023] also need a spatial discretization over the model to numerically solve the dynamics equation. Those prior arts sample the model based on the learned density distribution. Doing so could result in sparsely sampled regions, especially for objects with thin parts, and potentially affect the simulation quality e.g., see Fig. 3.

4.2 Training

While the sampled kernels well represent the boundary of the objects and offer a simulation-ready discretization, their visual attributes or material parameters (e.g., diffuse, specular, roughness) have yet to be determined. Without them, high-quality rendering results are not possible. We leverage the differentiable 3DGS pipeline to optimize the appearance of every Gaussian kernel. All Gaussian kernels are first shaded with their corresponding material parameters (Eq. (5)) and are then splatted to a rendered image. Comparing it with the training view gives a loss back-propagated to update the corresponding parameters of Gaussian kernels. Specifically, the trainable parameters for each kernel p are opacity σ_p , covariance A_p and material $\{d_p, s_p, \rho_p, n_p\}$. During training we consider the kernel center x_p as fixed to retain the discretization for the simulation. The loss is defined as:

$$\mathcal{L} = \mathcal{L}_{\text{color}} + \lambda_n \mathcal{L}_{\text{normal}} + \lambda_a \mathcal{L}_{\text{aniso}} + \lambda_v \mathcal{L}_{\text{vol}}, \quad (6)$$

where $\mathcal{L}_{\text{color}}$ is the color loss between render and training image; $\mathcal{L}_{\text{normal}}$ is normal consistency regularization adopted from Gaussian shader [Jiang et al. 2023]. The regularization term $\mathcal{L}_{\text{aniso}}$ is designed to prevent Gaussian kernels from becoming excessively elongated or compressed and potentially producing artifacts under large deformations. It is defined as:

$$\mathcal{L}_{\text{aniso}} = \frac{1}{|\mathcal{P}|} \sum_{p \in \mathcal{P}} \max \left\{ \frac{S_p^1}{S_p^2} - a, 0 \right\}, \quad (7)$$

where a is a ratio threshold and $S_p = \{S_p^1, S_p^2, S_p^3\}$ are the scalings of Gaussian kernels with S_p^1 being the largest scaling and S_p^3 being the smallest scaling. Note that as the shading normal is based on the minimal axis of Gaussian kernels, we do not constrain the minimal axis in the anisotropy loss. Otherwise, a spherical ellipsoid will result in normal ambiguity. We further encourage all Gaussian kernels to be relatively same-size by applying a regularization term:

$$\mathcal{L}_{\text{vol}} = \frac{1}{|\mathcal{P}|} \sum_{p \in \mathcal{P}} \left(\frac{S_p^1 S_p^2 S_p^3}{\frac{1}{|\mathcal{P}|} \sum_{q \in \mathcal{P}} S_q^1 S_q^2 S_q^3} - 1 \right)^2. \quad (8)$$

We set $a = 1.1$, $\lambda_n = 0.2$, $\lambda_a = 10$, and $\lambda_v = 10$ in our experiments.

4.3 Position Based Fluids

We employ the position-based fluids (PBF) [Macklin and Müller 2013] as our Lagrangian fluid synthesizer. To enforce the fluid incompressibility, PBF imposes a density constraint C_i^ρ on each particle, maintaining the integrated density ρ_i computed by the SPH kernel as:

$$C_i^\rho = \frac{\rho_i}{\rho_0} - 1 = \sum_j \frac{m_j}{\rho_0} W(\mathbf{p}_i - \mathbf{p}_j) - 1, \quad (9)$$

where m_j is the mass of particle j . \mathbf{p}_i is the position of particle i , and W is the SPH kernel function. The constraint Jacobian is:

$$\nabla_{\mathbf{p}_k} C_i^\rho = \begin{cases} \sum_j \frac{m_j}{\rho_0} \nabla_{\mathbf{p}_i} W(\mathbf{p}_i - \mathbf{p}_j), & k = i \\ \frac{m_j}{\rho_0} \nabla_{\mathbf{p}_j} W(\mathbf{p}_i - \mathbf{p}_j), & k = j. \end{cases} \quad (10)$$

GSP also includes a position-based tension model [Xing et al. 2022] to better capture the dynamics of the fluid surface. We first detect whether a particle (i.e., a Gaussian kernel) is on the fluid surface based on occlusion estimation. Specifically, we encapsulate a particle with a spherical cover or screen. Each of its neighboring particles generates a projection on the screen (because a particle has a finite volume). The particle is considered on the fluid surface if the total projection area from its neighbors is below a given threshold. Tensions tends to minimize surface area. Therefore, PBF applies an area constraint to each surface particle to minimize the local surface area nearby.

We start by calculating the normal \mathbf{n}_i of surface particles i as:

$$\mathbf{n}_i = \text{normalize}(-\nabla_{\mathbf{p}_i} C_i^\rho), \quad (11)$$

where $C_i^\rho = 0$ indicates the particle is inside the fluid, and $C_i^\rho = -1$ indicates it is outside. After that, we project the neighboring surface particles onto a plane perpendicular to \mathbf{n}_i and triangularize the

plane. The area constraint can then be built as:

$$C_i^A = \sum_{t \in T(i)} \frac{1}{2} \|(\mathbf{p}_{t^2} - \mathbf{p}_{t^1}) \times (\mathbf{p}_{t^3} - \mathbf{p}_{t^1})\| \quad (12)$$

where $T(i)$ is the set of neighboring triangles for particle i . To promote a more uniform particle distribution, additional distance constraints are introduced to push apart particles that are too close to each other:

$$C_{ij}^D = \min \{0, \|\mathbf{p}_i - \mathbf{p}_j\| - d_0\}, \quad (13)$$

where d_0 is the distance threshold. The Jacobian of these constraints are:

$$\begin{aligned} \nabla_{t^1} C_t^A(\mathbf{p}) &= \frac{1}{2} \frac{(\mathbf{p}_{t^2} - \mathbf{p}_{t^1}) \times (\mathbf{p}_{t^3} - \mathbf{p}_{t^1})}{\|(\mathbf{p}_{t^2} - \mathbf{p}_{t^1}) \times (\mathbf{p}_{t^3} - \mathbf{p}_{t^1})\|} \times (\mathbf{p}_{t^3} - \mathbf{p}_{t^2}), \\ \nabla_{t^2} C_t^A(\mathbf{p}) &= \frac{1}{2} \frac{(\mathbf{p}_{t^3} - \mathbf{p}_{t^2}) \times (\mathbf{p}_{t^1} - \mathbf{p}_{t^2})}{\|(\mathbf{p}_{t^3} - \mathbf{p}_{t^2}) \times (\mathbf{p}_{t^1} - \mathbf{p}_{t^2})\|} \times (\mathbf{p}_{t^1} - \mathbf{p}_{t^3}), \\ \nabla_{t^3} C_t^A(\mathbf{p}) &= \frac{1}{2} \frac{(\mathbf{p}_{t^1} - \mathbf{p}_{t^3}) \times (\mathbf{p}_{t^2} - \mathbf{p}_{t^3})}{\|(\mathbf{p}_{t^1} - \mathbf{p}_{t^3}) \times (\mathbf{p}_{t^2} - \mathbf{p}_{t^3})\|} \times (\mathbf{p}_{t^2} - \mathbf{p}_{t^1}), \\ \nabla_i C_{ij}^D(\mathbf{p}) &= \begin{cases} \mathbf{0}, & \|\mathbf{p}_i - \mathbf{p}_j\| > d_0, \\ \frac{\mathbf{p}_i - \mathbf{p}_j}{\|\mathbf{p}_i - \mathbf{p}_j\|}, & \text{Others.} \end{cases} \\ \nabla_j C_{ij}^D(\mathbf{p}) &= \begin{cases} \mathbf{0}, & \|\mathbf{p}_i - \mathbf{p}_j\| > d_0, \\ \frac{\mathbf{p}_j - \mathbf{p}_i}{\|\mathbf{p}_i - \mathbf{p}_j\|}, & \text{Others.} \end{cases} \end{aligned} \quad (14)$$

4.4 Rendering

The rendering of the dynamic scene reuses the existing 3DGS pipeline. For dynamic solids, we first transform each solid Gaussian kernel from rest positions \mathbf{x}_p to deformed positions \mathbf{x}_p^t where t indicates the time step index. We directly place these kernels at deformed positions. For a kernel with deformation gradient F_p , its covariance A_p^t and normal \mathbf{n}_p^t after deformation is updated by:

$$A_p^t = F_p A_p F_p^T, \text{ and } \mathbf{n}_p^t = \frac{F_p^{-T} \mathbf{n}_p}{\|F_p^{-T} \mathbf{n}_p\|}. \quad (15)$$

We then shade the deformed Gaussian kernels $\{\mathbf{x}_p^t, \sigma_p, A_p^t, \mathbf{n}_p^t\}$ with material $\{d_p, s_p, \rho_p\}$ i.e., Eq. (5) and splat them into an image \mathbf{c}^{bg} . The dynamic particle-based fluids are rendered with ellipsoids splatting [Macklin and Müller 2013], which is inherently compatible with the existing 3DGS pipeline. We begin by generating fluid Gaussian kernels at each fluid particle. The initial covariance A_p of each kernel is determined by the particle radius. The normal \mathbf{n}_p adopts the surface normal of the nearest surface fluid particle from PBF simulation. We then align the minimal axis of the Gaussian kernel with \mathbf{n}_p by a single rotation and correspondingly adjust the initial covariance.

We proceed to set up the appearance material for each fluid Gaussian kernel. It is known that fluid's appearance exhibits strong reflection and refraction effects. We employ the current PBR workflow to model the reflection, which adopts the same formula of Eq. (5). We set a specular material ($s_p = 1$, $\rho_p = 0.05$ in our experiments) for all fluid kernels to imitate reflective behavior. The refraction needs careful treatment, which we model into a thickness-dependent diffuse

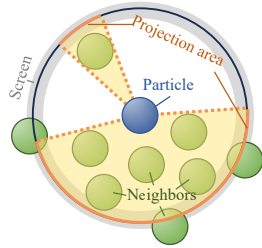


Fig. 4. **Detection of surface particles.** An interior particle is detected if its screen is widely shadowed by its neighbors. A boundary particle is detected if at least one part of the particle's screen is not shadowed.

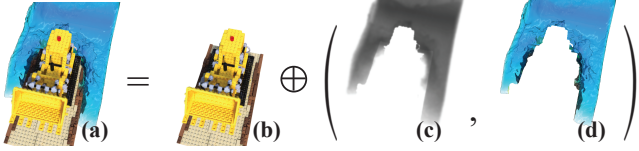


Fig. 5. **GSP rendering.** GSP synthesizes high-quality images corresponding to dynamically interacting fluids and solids. (a) The final rendered image combining rendered solids and fluids; (b) The rendering result of deforming solids; (c) The fluid thickness by additive splatting, where the darker color indicates the higher thickness; (d) The rendered dynamic fluids which is not occluded by solids.

color d_p . As the fluid thickness increases, the absorption of light within the fluid intensifies, resulting in reduced visibility for objects behind. Conversely, when there is less fluid present, it exhibits a more transparent appearance. The fluid thickness τ comes from the modified splatting pipeline, with the alpha blending replaced by additive blending. The refraction color d_p is then represented by Beer’s Law [Swinehart 1962]:

$$d_p = e^{-k\tau_p} c_p^{\text{bg}}. \quad (16)$$

Here, the absorption coefficient k is defined differently for each color channel, τ_p, c_p^{bg} is the fluid thickness and background back-projected to each Gaussian kernel respectively. Note that for background back-projection, a distortion βn_p is added to mimic the change of light path. Opacity σ_p is set to 1 as most of transmission and refraction has already been modeled into d_p . We finally shade all fluid Gaussian kernels $\{x^t, \sigma_p, A_p^t, n_p^t d_p, s_p, \rho_p\}$ and splat them to the fluid rendering result c^{fluid} with Gaussian splatting. The final rendering result is achieved by combining the c^{bg} and c^{fluid} , as shown in Fig. 5.

4.5 Inpainting

Displaced object exposes unseen areas that were originally covered to the camera. Since they are not present in the input image, 3DGS is unable to recover the color and texture information of these areas, leading to black smudges and dirty textures in the result. GSP remedies this issue using an inpainting trick. First, we remove all the Gaussian kernels of the object that may be displaced. We then use LaMa [Suvorov et al. 2022] to inpaint the rendered results, noting the new colors of pixels originally in spots and assigning them to the first Gaussian kernel encountered by the rays emitted from these pixels. We average the recorded colors on all noted Gaussian kernels for their diffuse color, set their opacity to 1, and their specular color to $\mathbf{0}$ to prevent highlights. The inpainted 3DGS rendering becomes much improved, as shown in Fig. 6.

5 EXPERIMENTS

We implemented GSP pipeline using Python, C++ and CUDA on a desktop PC equipped with a 12-core Intel i7-12700F CPU and an NVIDIA RTX 3090 GPU. Specifically, for rendering part, we ported the published implementation of Gaussian shader [Jiang et al. 2023] and integrated our fluid rendering using PyTorch [Imambi et al. 2021]. PBD/PBF engine was implemented with CUDA, and we also

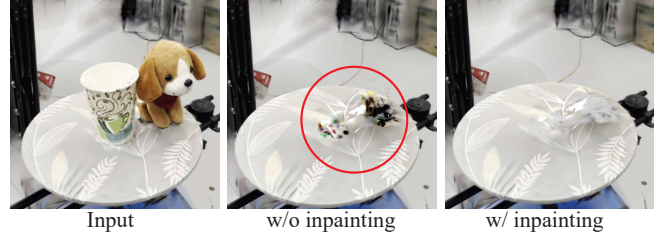


Fig. 6. **3DGS inpainting.** In this indoor scene, both the paper cup and the stuffed toy dog are segmented from the input image (left). 3DGS leaves empty spots and dirty textures blended from irrelevant kernels, as highlighted in the middle figure. Applying the inpainting with generative AI [Suvorov et al. 2022] ameliorates this issue (right).



Fig. 7. **Anisotropy regularization.** Anisotropy regularization effectively maintains rendering quality under large deformations. Without the regularization term, 3DGS tends to generate fuzzy and spiky artifacts, especially near the surface of the model (left). When the regularization is applied, image quality is greatly improved with correct specular effects.

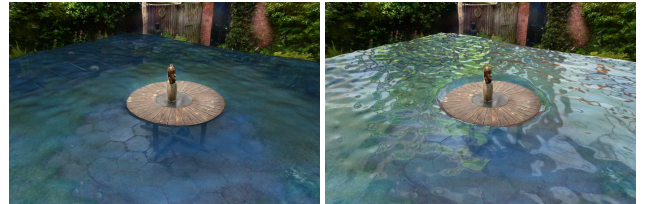


Fig. 8. **Ablation study of specular.** We demonstrate the impact of specular highlights on the quality of rendering. On the left is a fluid rendered with diffuse color only; On the right, surface reflective specular are added, which exhibits a more realistic and dynamic fluid.

group independent constraints in colors to efficiently parallelize the constraint projections on the GPU. We set the simulation time step as 0.005 seconds throughout the simulations. In our PBD solver, we used 10 iterations for fluids and 50 iterations for solids for our experiments, since mass particles on the solid models are stronger coupled than the ones in the fluid. During the PBF simulation, the surface particles of fluids are updated every two time steps. 3DGS is originally designed for view synthesis. 3DGS obtained from a static scene produces low-quality renders when Gaussian kernels undergo large rotational deformations. The anisotropy regularization is effective against this limitation as shown Fig. 7. Detailed statistics regarding the experiment settings and timings are reported in Tab. 1. Most experiments can also be found in the supplementary video.

To show the importance of specular highlights in fluid rendering, we show a side-by-side comparison in a 3DGS scene. As shown in

Table 1. **Time performance.** We report detailed time statistics for experiments reported in the paper. **NeuS** gives the total time of mesh reconstruction. **Train** is the total time of training 3DGS. Both of the above measurements are in hours. However, all subsequent time-related evaluations are presented in seconds. **# BG**, **# Solids** and **# Fluids** represent the number of Gaussian kernels for the background, the foreground solid, and the fluid, respectively. **Sim** is the total time of simulation per time step. **Tension** represents the time taken for each surface particle detection. **Render** represents the total rendering time. **Render BG**, **Render solids** and **Render fluids** indicate the time spent on rendering the background, solids and fluids. Some experiments incorporates some specific settings, In the **Book & Lego** case, we only account for the simulation and rendering performance after the book transforms into water and the Lego excavator falls. **Train** is the sum of the book and the excavator. **# Fluids** is the counts of Gaussian kernels of the book, and **# solids** is the counts of Gaussian kernels of the excavator. In the **Can**, since the solid is completely fixed, only the fluid is involved in the **Sim**.

Scene	NeuS	Train	# BG	# Solids	# Fluids	Sim	Tension	Render BG	Render solids	Render fluids	Render
Chair (Fig. 9)	0.44 h	0.70 h	0	315K	300K	5.4 s	1.1 s	0 s	0.039 s	0.059 s	0.098 s
Garden (Fig. 10)	0.67 h	2.21 h	2.27M	450K	0 ~ 614K	10.3 s	2.3 s	0.023 s	0.069 s	0.103 s	0.195 s
Book & Lego (Fig. 11)	1.03 h	1.43 h	300K	247K 334K	0 247K	3.7 s	0.8 s	0.019 s	0.051 s	0.046 s	0.116 s
Can (Fig. 12)	0.43 h	1.36 h	1.19M	390K	0 ~ 254K	1.6 s	0.8 s	0.020 s	0.025 s	0.047 s	0.092 s
Cup & dog (Fig. 13)	0.74 h	0.74 h	310K	156K ~ 16k	0 ~ 170K	2.1 s	0.6 s	0.019 s	0.024 s	0.041 s	0.083 s
Astronaut (Fig. 14)	0.57 h	0.56 h	0	0	145K	0.8 s	0.6 s	0 s	0 s	0.040 s	0.040 s

Fig. 8, we compare fluids rendered using purely diffuse materials with those that incorporated specular reflections. The fluids without specular reflection appear almost smoke-like, while the inclusion of specular term significantly enhances the realism of the fluids.

We test GSP in a diverse set of experiments. A “warm-up” test is shown in Fig. 9, where a soft chair from NeRF synthetic datasets [Mildenhall et al. 2020] falls into a pool, illustrating the two-way coupling between deformable solids and fluids. The chair undergoes deformation, floats due to buoyancy, and creates fluid ripples as a result. Fig. 10 showcases another fluid-solid interaction test. The garden scene is sourced from the Mip-NeRF 360 [Barron et al. 2022] dataset. The foreground objects consist of a fixed table and a potted plant. We pour water into the garden slowly. The water rises up and eventually sinks the table, and sweeps the plant.

GSP has a semantic segmentation module. Therefore, the user is able to freely manipulate the models in the scene. Furthermore, since everything is represented as Gaussian particles, GSP allows the user to transform the state of the model. An example is shown in Fig. 11. In this indoor scene, three stacking books are isolated and segmented before training the 3DGS. The user transforms them from solid objects to fluid and instantly creates an in-door pool. A pre-trained Lego excavator falls into the “pool”. It then floats due to the buoyancy. Another similar experiment is reported in Fig. 13. The scene includes a round white table, on which a paper cup and a stuffed toy dog are placed. Water is poured into the cup. The state of toy dog and the cup are changed to water, and splashes on the desk. As mentioned, we use LaMA to inpaint the table texture so that the user does not observe rendering artifacts when the liquefied cup and toy dog splashes away.

Our fluid simulator can also capture the surface tension within the PBD framework. This enables realistic low-volume fluid-solid interaction. As shown in Fig. 12, droplets of water continuously drip onto the top of the can until they reaches the capacity and

overflow. The surface tension of the liquid causes the droplets to gradually aggregate at the surface. As more droplets fall onto the liquid surface, they rise above the edge of the can. Eventually, the accumulated water exceeds the limit of surface tension and spills over, resulting in overflow.

Fig. 14 showcases another interesting use of GSP, where the user applies Trisolarians’ black magic on an astronaut. The astronaut is struck by the magic and is transformed to water. It finally collapses into a water ball in a zero-gravity space due to the presence of surface tension.

6 CONCLUSION

Gaussian Splashing is a novel pipeline combining versatile position-based dynamics with 3DGS. The principle design philosophy of GSP is to harness the consistency of volume particle-based discretization to enable integrated processing of various 3D graphics and vision tasks, such as 3D reconstruction, deformable simulation, fluid dynamics, and rendering from new camera angles. While the concept is straightforward, building GSP involves significant research and engineering efforts. The presence of fluid complicates the 3DGS processing due to the specular highlights at the fluid surface; Fluid-solid coupling resorts to accurate surface information; Large deformation on the solid object generates defective rendering; Displaced models also leave empty regions that the input images fail to capture. We overcome those difficulties by systematically integrating and adapting a collection of state-of-the-art technologies into the framework. As a result, GSP enables realistic view synthesis not only under novel camera poses but also with novel physically-based fluid/solid dynamics or even novel object state transform. It should be noted that incorporating physically-based fluid dynamics in NeRF/3DGS has not been explored previously. The primary contribution of this work is to showcase the feasibility of building a unified framework for integrated physics and learning-based 3D reconstruction. GSP

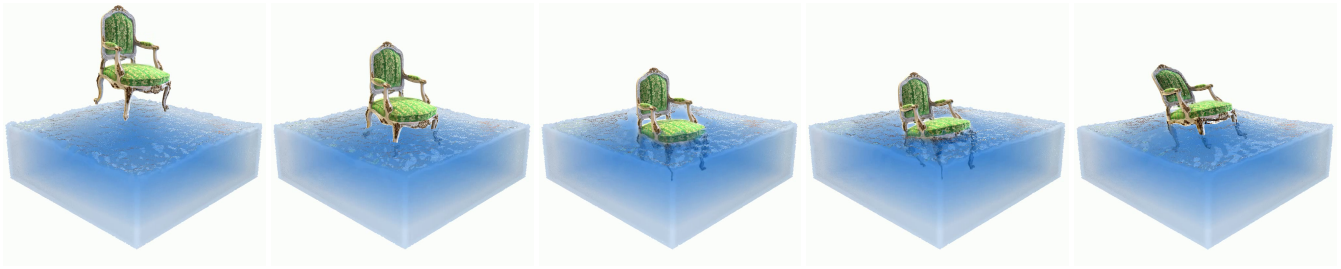


Fig. 9. **Chair.** A soft chair fell into the pool, causing deformation and ripples.



Fig. 10. **Flooding garden.** Waters leak into the garden and submerge the table. As the water level goes up, the surface gets more vibrant and washes the potted plant away.

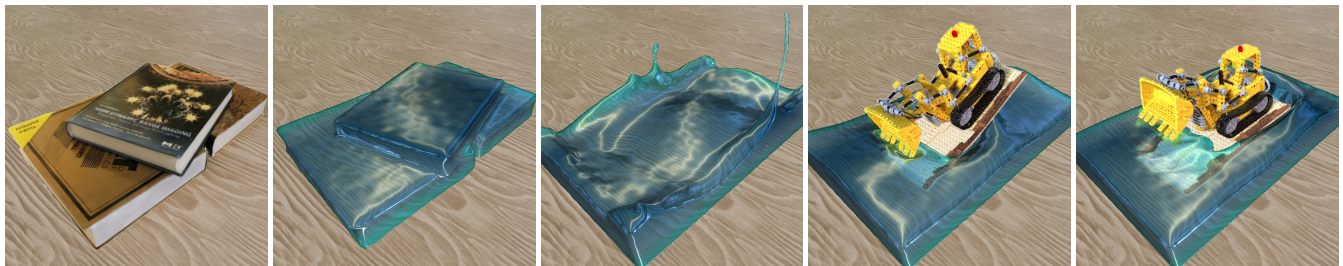


Fig. 11. **From books to pool.** Three books stack on the desk. They are isolated and segmented in GSP. The user switches their solid Gaussians to fluid Gaussians to make an indoor pool and drops a LEGO excavator into it.



Fig. 12. **Water droplets on can.** Droplets of water fall onto the surface of a soda can, coalesce due to surface tension and gradually overflow.

still has many limitations. For instance, PBD is known to be less physically accurate. It may be worth generalizing PBD with other meshless simulation methods. The fluid rendering in GSP in its current form is far from perfect – ellipsoid splatting is an ideal candidate for position-based fluid but does not physically handle

refraction. PBF may need a large number of fluid particles, which negatively impacts the rendering efficiency.

REFERENCES

Marc Alexa, Markus Gross, Mark Pauly, Hanspeter Pfister, Marc Stamminger, and Matthias Zwicker. 2004. Point-based computer graphics. In *ACM SIGGRAPH 2004*

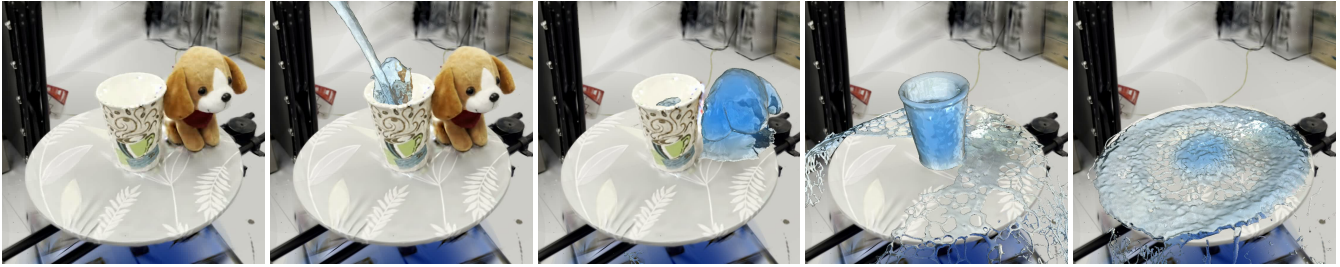


Fig. 13. “Everything is water”. Pouring water into the paper cup on the table and transforming the cup and a dog toy into water. The water spills out.

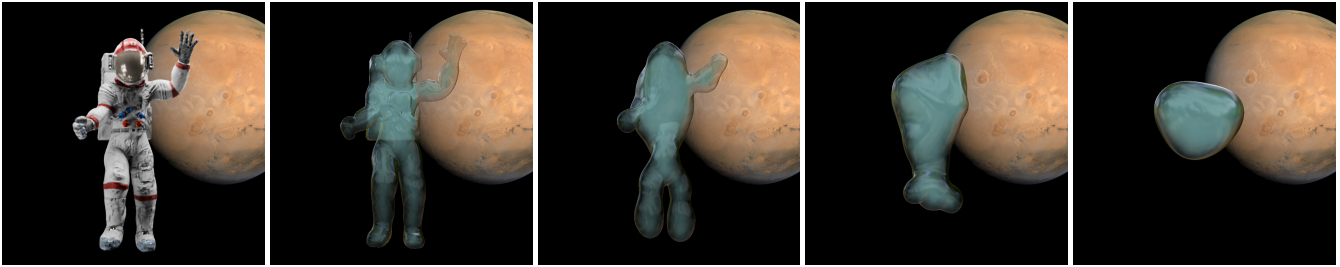


Fig. 14. **Black magic**. An astronaut in the space struck by the black magic of the Trisolarians, and get transformed into a water sphere.

Course Notes. 7–es.

- Chong Bao, Yinda Zhang, Bangbang Yang, Tianxing Fan, Zesong Yang, Hujun Bao, Guofeng Zhang, and Zhaopeng Cui. 2023. Sine: Semantic-driven nerf editing with prior-guided editing field. In *Proceedings of the IEEE/CVF Conference on Computer Vision and Pattern Recognition*. 20919–20929.
- Jonathan T Barron and Jitendra Malik. 2014. Shape, illumination, and reflectance from shading. *IEEE transactions on pattern analysis and machine intelligence* 37, 8 (2014), 1670–1687.
- Jonathan T. Barron, Ben Mildenhall, Dor Verbin, Pratul P. Srinivasan, and Peter Hedman. 2022. Mip-NeRF 360: Unbounded Anti-Aliased Neural Radiance Fields. *CVPR* (2022).
- Markus Becker and Matthias Teschner. 2007. Weakly compressible SPH for free surface flows. In *Proceedings of the 2007 ACM SIGGRAPH/Eurographics Symposium on Computer Animation* (San Diego, California) (SCA '07). Eurographics Association, Goslar, DEU, 209–217.
- Sai Bi, Zexiang Xu, Pratul Srinivasan, Ben Mildenhall, Kalyan Sunkavalli, Miloš Hašan, Yannick Hold-Geoffroy, David Kriegman, and Ravi Ramamoorthi. 2020. Neural reflectance fields for appearance acquisition. *arXiv preprint arXiv:2008.03824* (2020).
- Mark Boss, Raphael Braun, Varun Jampani, Jonathan T Barron, Ce Liu, and Hendrik Lensch. 2021a. Nerf: Neural reflectance decomposition from image collections. In *Proceedings of the IEEE/CVF International Conference on Computer Vision*. 12684–12694.
- Mark Boss, Varun Jampani, Raphael Braun, Ce Liu, Jonathan Barron, and Hendrik Lensch. 2021b. Neural-pil: Neural pre-integrated lighting for reflectance decomposition. *Advances in Neural Information Processing Systems* 34 (2021), 10691–10704.
- Robert Bridson. 2007. Fast Poisson disk sampling in arbitrary dimensions. *SIGGRAPH sketches* 10, 1 (2007), 1.
- Giang Bui, Truc Le, Brittany Morago, and Ye Duan. 2018. Point-based rendering enhancement via deep learning. *The Visual Computer* 34 (2018), 829–841.
- Ho Kei Cheng, Seoung Wug Oh, Brian Price, Joon-Young Lee, and Alexander Schwing. 2023. Putting the Object Back into Video Object Segmentation. In *arXiv*.
- H Childs, T Kuhlen, and F Marton. 2012. Auto splats: Dynamic point cloud visualization on the gpu. In *Proc. Eurographics Symp. Parallel Graph. Vis.* 1–10.
- Jiahua Dong and Yu-Xiong Wang. 2023. ViCA-NeRF: View-Consistency-Aware 3D Editing of Neural Radiance Fields. In *Thirty-seventh Conference on Neural Information Processing Systems*.
- Yilun Du, Yanan Zhang, Hong-Xing Yu, Joshua B Tenenbaum, and Jiajun Wu. 2021. Neural radiance flow for 4d view synthesis and video processing. In *2021 IEEE/CVF International Conference on Computer Vision (ICCV)*. IEEE Computer Society, 14304–14314.
- Bardienus P Duisterhof, Zhao Mandi, Yunchao Yao, Jia-Wei Liu, Mike Zheng Shou, Shuran Song, and Jeffrey Ichnowski. 2023. MD-Splatting: Learning Metric Deformation from 4D Gaussians in Highly Deformable Scenes. *arXiv preprint arXiv:2312.00583* (2023).
- Yutao Feng, Yintong Shang, Xuan Li, Tianjia Shao, Chenfanfu Jiang, and Yin Yang. 2023. PIE-NeRF: Physics-based Interactive Elastodynamics with NeRF. *arXiv:2311.13099* [cs.CV]
- Chen Gao, Ayush Saraf, Johannes Kopf, and Jia-Bin Huang. 2021. Dynamic view synthesis from dynamic monocular video. In *Proceedings of the IEEE/CVF International Conference on Computer Vision*. 5712–5721.
- Stephan J Garbin, Marek Kowalski, Matthew Johnson, Jamie Shotton, and Julien Valentin. 2021. Fastnerf: High-fidelity neural rendering at 200fps. In *Proceedings of the IEEE/CVF International Conference on Computer Vision*. 14346–14355.
- Jeffrey P Grossman and William J Dally. 1998. Point sample rendering. In *Rendering Techniques '98: Proceedings of the Eurographics Workshop in Vienna, Austria, June 29–July 1, 1998*. Springer, 181–192.
- Antoine Guédon and Vincent Lepetit. 2023. SuGaR: Surface-Aligned Gaussian Splatting for Efficient 3D Mesh Reconstruction and High-Quality Mesh Rendering. *arXiv preprint arXiv:2311.12775* (2023).
- Xiang Guo, Jiadao Sun, Yuchao Dai, Guanying Chen, Xiaoqing Ye, Xiao Tan, Errui Ding, Yumeng Zhang, and Jingdong Wang. 2023. Forward Flow for Novel View Synthesis of Dynamic Scenes. In *Proceedings of the IEEE/CVF International Conference on Computer Vision*. 16022–16033.
- Sagar Imambi, Kolla Bhanu Prakash, and GR Kanagachidambaresan. 2021. PyTorch. *Programming with TensorFlow: Solution for Edge Computing Applications* (2021), 87–104.
- Ajay Jain, Matthew Tancik, and Pieter Abbeel. 2021. Putting nerf on a diet: Semantically consistent few-shot view synthesis. In *Proceedings of the IEEE/CVF International Conference on Computer Vision*. 5885–5894.
- Kaiwen Jiang, Shu-Yu Chen, Feng-Lin Liu, Hongbo Fu, and Lin Gao. 2022. NeRFFaceEditing: Disentangled face editing in neural radiance fields. In *SIGGRAPH Asia 2022 Conference Papers*. 1–9.
- Yingwenqi Jiang, Jiadong Tu, Yuan Liu, Xifeng Gao, Xiaoxiao Long, Wenping Wang, and Yuexin Ma. 2023. GaussianShader: 3D Gaussian Splatting with Shading Functions for Reflective Surfaces. *arXiv:2311.17977* [cs.CV]
- Dahyun Kang, Daniel S Jeon, Hakyong Kim, Hyeonjoong Jang, and Min H Kim. 2021. View-dependent scene appearance synthesis using inverse rendering from light fields. In *2021 IEEE International Conference on Computational Photography (ICCP)*. IEEE, 1–12.
- Bernhard Kerbl, Georgios Kopanas, Thomas Leimkühler, and George Drettakis. 2023. 3D Gaussian Splatting for Real-Time Radiance Field Rendering. *ACM Transactions on Graphics* 42, 4 (July 2023). <https://repo-sam.inria.fr/fungraph/3d-gaussian-splatting/>
- Alexander Kirillov, Eric Mintun, Nikhila Ravi, Hanzi Mao, Chloe Rolland, Laura Gustafson, Tete Xiao, Spencer Whitehead, Alexander C Berg, Wan-Yen Lo, et al. 2023. Segment anything. *arXiv preprint arXiv:2304.02643* (2023).
- Marc Levoy and Turner Whitted. 1985. The use of points as a display primitive. (1985).

- Xuan Li, Yi-Ling Qiao, Peter Yichen Chen, Krishna Murthy Jatavallabhula, Ming Lin, Chenfanfu Jiang, and Chuang Gan. 2023. PAC-NeRF: Physics Augmented Continuum Neural Radiance Fields for Geometry-Agnostic System Identification. In *The Eleventh International Conference on Learning Representations*. <https://openreview.net/forum?id=tVkrbkz42vc>
- Zhengqi Li, Simon Niklaus, Noah Snavely, and Oliver Wang. 2021. Neural scene flow fields for space-time view synthesis of dynamic scenes. In *Proceedings of the IEEE/CVF Conference on Computer Vision and Pattern Recognition*. 6498–6508.
- Ruofan Liang, Huiting Chen, Chunlin Li, Fan Chen, Selvakumar Panneer, and Nandita Vijaykumar. 2023a. ENVIDR: Implicit Differentiable Renderer with Neural Environment Lighting. *arXiv preprint arXiv:2303.13022* (2023).
- Ruofan Liang, Jiahao Zhang, Haoda Li, Chen Yang, and Nandita Vijaykumar. 2022. Spidr: Sdf-based neural point fields for illumination and deformation. *arXiv preprint arXiv:2210.08398* (2022).
- Yiqing Liang, Numair Khan, Zhengqin Li, Thu Nguyen-Phuoc, Douglas Lanman, James Tompkin, and Lei Xiao. 2023b. GauFR: Gaussian Deformation Fields for Real-time Dynamic Novel View Synthesis. *arXiv:2312.11458* [cs.CV]
- Jia-Wei Liu, Yan-Pei Cao, Weijia Mao, Wenqiao Zhang, David Junhao Zhang, Jussi Keppo, Ying Shan, Xiaohu Qie, and Mike Zheng Shou. 2022. Devrf: Fast deformable voxel radiance fields for dynamic scenes. *Advances in Neural Information Processing Systems* 35 (2022), 36762–36775.
- Lingjie Liu, Jiatao Gu, Kyaw Zaw Lin, Tat-Seng Chua, and Christian Theobalt. 2020. Neural sparse voxel fields. *Advances in Neural Information Processing Systems* 33 (2020), 15651–15663.
- Yuan Liu, Peng Wang, Cheng Lin, Xiaoxiao Long, Jiepeng Wang, Lingjie Liu, Taku Komura, and Wenping Wang. 2023. NeRO: Neural Geometry and BRDF Reconstruction of Reflective Objects from Multiview Images. *arXiv preprint arXiv:2305.17398* (2023).
- Miles Macklin and Matthias Müller. 2013. Position based fluids. *ACM Transactions on Graphics (TOG)* 32, 4 (2013), 1–12.
- Miles Macklin and Matthias Müller. 2021. A constraint-based formulation of stable neo-hookean materials. In *Proceedings of the 14th ACM SIGGRAPH conference on motion, interaction and games*. 1–7.
- Miles Macklin, Matthias Müller, and Nuttapon Chentanez. 2016. XPBD: position-based simulation of compliant constrained dynamics. In *Proceedings of the 9th International Conference on Motion in Games*. 49–54.
- Ben Mildenhall, Pratul P. Srinivasan, Matthew Tancik, Jonathan T. Barron, Ravi Ramamoorthi, and Ren Ng. 2020. NeRF: Representing scenes as neural radiance fields for view synthesis. In *The European Conference on Computer Vision (ECCV)*.
- Joe J Monaghan. 1992. Smoothed particle hydrodynamics. *Annual review of astronomy and astrophysics* 30, 1 (1992), 543–574.
- Arthur Moreau, Jifei Song, Helisa Dharmo, Richard Shaw, Yiren Zhou, and Eduardo Pérez-Pellitero. 2023. Human Gaussian Splatting: Real-time Rendering of Animatable Avatars. *arXiv preprint arXiv:2311.17113* (2023).
- Matthias Müller and Nuttapon Chentanez. 2011. Solid simulation with oriented particles. In *ACM SIGGRAPH 2011 papers*. 1–10.
- Matthias Müller, Bruno Heidelberger, Marcus Hennix, and John Ratcliff. 2007. Position based dynamics. *Journal of Visual Communication and Image Representation* 18, 2 (2007), 109–118.
- Matthias Müller, Miles Macklin, Nuttapon Chentanez, Stefan Jeschke, and Tae-Yong Kim. 2020. Detailed rigid body simulation with extended position based dynamics. In *Computer graphics forum*, Vol. 39. Wiley Online Library, 101–112.
- Thomas Müller, Alex Evans, Christoph Schied, and Alexander Keller. 2022. Instant Neural Graphics Primitives with a Multiresolution Hash Encoding. *ACM Trans. Graph.* 41, 4, Article 102 (jul 2022), 15 pages. <https://doi.org/10.1145/3528223.3530127>
- Merlin Nimier-David, Delio Vicini, Tizian Zeltner, and Wenzel Jakob. 2019. Mitsuba 2: A retargetable forward and inverse renderer. *ACM Transactions on Graphics (TOG)* 38, 6 (2019), 1–17.
- Keunghong Park, Utkarsh Sinha, Jonathan T Barron, Sofien Bouaziz, Dan B Goldman, Steven M Seitz, and Ricardo Martin-Brualla. 2021a. Nerfies: Deformable neural radiance fields. In *Proceedings of the IEEE/CVF International Conference on Computer Vision*. 5865–5874.
- Keunghong Park, Utkarsh Sinha, Peter Hedman, Jonathan T Barron, Sofien Bouaziz, Dan B Goldman, Ricardo Martin-Brualla, and Steven M Seitz. 2021b. Hypernerf: A higher-dimensional representation for topologically varying neural radiance fields. *arXiv preprint arXiv:2106.13228* (2021).
- Yicong Peng, Yichao Yan, Shengqi Liu, Yuhao Cheng, Shanyan Guan, Bowen Pan, Guangtao Zhai, and Xiaokang Yang. 2022. CageNeRF: Cage-based Neural Radiance Field for Generalized 3D Deformation and Animation. In *Advances in Neural Information Processing Systems*, S. Koyejo, S. Mohamed, A. Agarwal, D. Belgrave, K. Cho, and A. Oh (Eds.), Vol. 35. Curran Associates, Inc., 31402–31415. https://proceedings.neurips.cc/paper_files/paper/2022/file/cb78e6b5246b03e0b82b4acc8b11cc21-Paper-Conference.pdf
- Ruggero Pintus, Enrico Gobbetti, and Marco Agus. 2011. Real-time rendering of massive unstructured raw point clouds using screen-space operators. In *Proceedings of the 12th International conference on Virtual Reality, Archaeology and Cultural Heritage*. 105–112.
- Albert Pumarola, Enric Corona, Gerard Pons-Moll, and Francesc Moreno-Noguer. 2021. D-nerf: Neural radiance fields for dynamic scenes. In *Proceedings of the IEEE/CVF Conference on Computer Vision and Pattern Recognition*. 10318–10327.
- Yi-Ling Qiao, Alexander Gao, Yiran Xu, Yue Feng, Jia-Bin Huang, and Ming C Lin. 2023. Dynamic mesh-aware radiance fields. In *Proceedings of the IEEE/CVF International Conference on Computer Vision*. 385–396.
- Barbara Solenthaler and Renato Pajarola. 2009. Predictive-corrective incompressible SPH. In *ACM SIGGRAPH 2009 papers*. 1–6.
- Pratul P Srinivasan, Boyang Deng, Xiuming Zhang, Matthew Tancik, Ben Mildenhall, and Jonathan T Barron. 2021. Nerv: Neural reflectance and visibility fields for relighting and view synthesis. In *Proceedings of the IEEE/CVF Conference on Computer Vision and Pattern Recognition*. 7495–7504.
- Roman Suvorov, Elizaveta Logacheva, Anton Mashikhin, Anastasia Remizova, Arsenii Ashukha, Aleksei Silvestrov, Naejin Kong, Harshith Goka, Kiwoong Park, and Victor Lempitsky. 2022. Resolution-robust large mask inpainting with fourier convolutions. In *Proceedings of the IEEE/CVF winter conference on applications of computer vision*. 2149–2159.
- Donald F Swinehart. 1962. The beer-lambert law. *Journal of chemical education* 39, 7 (1962), 339.
- Edgar Tretschk, Ayush Tewari, Vladislav Golyanik, Michael Zollhöfer, Christoph Lassner, and Christian Theobalt. 2021. Non-rigid neural radiance fields: Reconstruction and novel view synthesis of a dynamic scene from monocular video. In *Proceedings of the IEEE/CVF International Conference on Computer Vision*. 12959–12970.
- Wladimir J. van der Laan, Simon Green, and Miguel Sainz. 2009. Screen space fluid rendering with curvature flow. In *Proceedings of the 2009 Symposium on Interactive 3D Graphics and Games (Boston, Massachusetts) (ISD '09)*. Association for Computing Machinery, New York, NY, USA, 91–98. <https://doi.org/10.1145/1507149.1507164>
- Peng Wang, Lingjie Liu, Yuan Liu, Christian Theobalt, Taku Komura, and Wenping Wang. 2021. NeuS: Learning Neural Implicit Surfaces by Volume Rendering for Multi-view Reconstruction. *NeurIPS* (2021).
- Chung-Yi Weng, Brian Curless, Pratul P Srinivasan, Jonathan T Barron, and Ira Kemelmacher-Shlizerman. 2022. Humannerf: Free-viewpoint rendering of moving people from monocular video. In *Proceedings of the IEEE/CVF conference on computer vision and pattern recognition*. 16210–16220.
- Guanjun Wu, Taoran Yi, Jiemin Fang, Lingxi Xie, Xiaopeng Zhang, Wei Wei, Wenyu Liu, Qi Tian, and Xinggang Wang. 2023. 4d gaussian splatting for real-time dynamic scene rendering. *arXiv preprint arXiv:2310.08528* (2023).
- Wenqi Xian, Jia-Bin Huang, Johannes Kopf, and Changil Kim. 2021. Space-time neural irradiance fields for free-viewpoint video. In *Proceedings of the IEEE/CVF Conference on Computer Vision and Pattern Recognition*. 9421–9431.
- Tianyi Xie, Zeshun Zong, Yuxing Qiu, Xuan Li, Yutao Feng, Yin Yang, and Chenfanfu Jiang. 2023. PhysGaussian: Physics-Integrated 3D Gaussians for Generative Dynamics. *arXiv preprint arXiv:2311.12198* (2023).
- Jingrui Xing, Liangwang Ruan, Bin Wang, Bo Zhu, and Baoquan Chen. 2022. Position-Based Surface Tension Flow. *ACM Trans. Graph.* 41, 6, Article 244 (nov 2022), 12 pages. <https://doi.org/10.1145/3550454.3555476>
- Qiangeng Xu, Zexiang Xu, Julien Philip, Sai Bi, Zhixin Shu, Kalyan Sunkavalli, and Ulrich Neumann. 2022. Point-nerf: Point-based neural radiance fields. In *Proceedings of the IEEE/CVF Conference on Computer Vision and Pattern Recognition*. 5438–5448.
- Tianhan Xu and Tatsuya Harada. 2022. Deforming Radiance Fields with Cages. In *ECCV*.
- Yuelang Xu, Benwang Chen, Zhe Li, Hongwen Zhang, Lizhen Wang, Zerong Zheng, and Yebin Liu. 2023. Gaussian Head Avatar: Ultra High-fidelity Head Avatar via Dynamic Gaussians. *arXiv:2312.03029* [cs.CV]
- Zhenpei Yang, Yuning Chai, Dragomir Anguelov, Yin Zhou, Pei Sun, D Erhan, Sean Rafferty, and Henrik Kretschmar. 2020. Surfelfan: Synthesizing realistic sensor data for autonomous driving. 2020 IEEE. In *CVF Conference on Computer Vision and Pattern Recognition (CVPR)*. 11115–11124.
- Zeyu Yang, Hongye Yang, Zijie Pan, Xiatian Zhu, and Li Zhang. 2023. Real-time photo-realistic dynamic scene representation and rendering with 4d gaussian splatting. *arXiv preprint arXiv:2310.10642* (2023).
- Alex Yu, Ruilong Li, Matthew Tancik, Hao Li, Ren Ng, and Angjoo Kanazawa. 2021. Plenotrees for real-time rendering of neural radiance fields. In *Proceedings of the IEEE/CVF International Conference on Computer Vision*. 5752–5761.
- Yu-Jie Yuan, Yu-Kun Lai, Yi-Hua Huang, Leif Kobbelt, and Lin Gao. 2022a. Neural radiance fields from sparse RGB-D images for high-quality view synthesis. *IEEE Transactions on Pattern Analysis and Machine Intelligence* (2022).
- Yu-Jie Yuan, Yang-Tian Sun, Yu-Kun Lai, Yuewen Ma, Rongfei Jia, and Lin Gao. 2022b. NeRF-editing: geometry editing of neural radiance fields. In *Proceedings of the IEEE/CVF Conference on Computer Vision and Pattern Recognition*. 18353–18364.
- Kai Zhang, Fujun Luan, Qianqian Wang, Kavita Bala, and Noah Snavely. 2021a. Physg: Inverse rendering with spherical gaussians for physics-based material editing and relighting. In *Proceedings of the IEEE/CVF Conference on Computer Vision and Pattern Recognition*. 5453–5462.

- Xiuming Zhang, Pratul P Srinivasan, Boyang Deng, Paul Debevec, William T Freeman, and Jonathan T Barron. 2021b. Nerfactor: Neural factorization of shape and reflectance under an unknown illumination. *ACM Transactions on Graphics (ToG)* 40, 6 (2021), 1–18.
- Wojciech Zielonka, Timur Bagautdinov, Shunsuke Saito, Michael Zollhöfer, Justus Thies, and Javier Romero. 2023. Drivable 3d gaussian avatars. *arXiv preprint arXiv:2311.08581* (2023).
- Matthias Zwicker, Hanspeter Pfister, Jeroen Van Baar, and Markus Gross. 2001. Surface splatting. In *Proceedings of the 28th annual conference on Computer graphics and interactive techniques*. 371–378.